ACS central science

http://pubs.acs.org/journal/acscii

Research Article

Inhibiting Ferroptosis through Disrupting the NCOA4–FTH1 Interaction: A New Mechanism of Action

Yuying Fang, Xiucai Chen, Qingyun Tan, Huihao Zhou, Jun Xu,* and Qiong Gu*

Cite This: *ACS Cent. Sci.* 2021, 7, 980–989

Read Online

ACCESS | Metrics & More | Article Recommendations | Supporting Information

ABSTRACT: Ferroptosis is an iron-dependent form of oxidative cell death, and the inhibition of ferroptosis is a promising strategy with which to prevent and treat neurological diseases. Herein we report a new ferroptosis inhibitor **9a** with a novel mechanism of action. It is demonstrated that nuclear receptor coactivator 4 (NCOA4), a cargo receptor for ferritinophagy, is the target of **9a**. Compound **9a** blocks ferroptosis by reducing the amount of bioavailable intracellular ferrous iron through disrupting the NCOA4–FTH1 protein–protein interaction. Further studies indicate that **9a** directly binds to recombinant protein NCOA4$^{383-522}$ and effectively blocks the NCOA4$^{383-522}$–FTH1 interaction. In a rat model of ischemic stroke, **9a** significantly ameliorates the ischemic-refusion injury. With the first ligand **9a**, this work reveals that NCOA4 is a promising drug target. Additionally, **9a** is the first NCOA4–FTH1 interaction inhibitor. This work paves a new road to the development of ferroptosis inhibitors against neurological diseases.

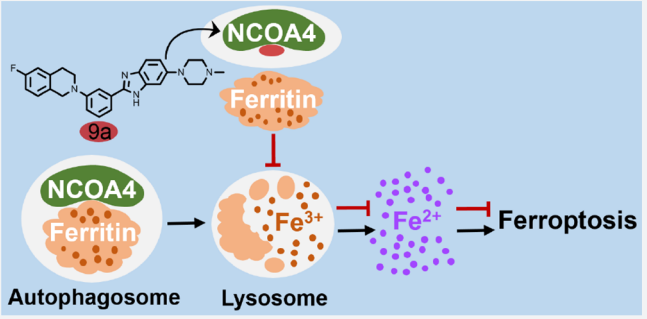

INTRODUCTION

Ferroptosis, a new type of programmed cell death, is characterized by excessive iron-dependent lipid peroxidation.[1,2] In the presence of ferrous iron, the abnormal accumulation of lipid hydroperoxides results in membrane destruction and irreversible cell death.[3] Glutathione peroxidase 4 (GPX4), a glutathione (GSH)-dependent selenoenzyme, plays a crucial role in preventing ferroptosis by reducing toxic lipid hydroperoxides to nontoxic lipid alcohols.[4,5] When the enzymatic activity of GPX4 is inhibited, lipid hydroperoxides accumulate significantly, leading to ferroptosis. Cysteine, the rate-limiting substrate for GSH synthesis, is obtained primarily from extracellular cystine through the cystine–glutamate antiporter system x_c^--mediated transport.[6] Consequently, the inhibition of system x_c^- or the inactivation or depletion of GPX4 can induce ferroptosis.[4,7,8]

Intracellular redox-active iron can promote the production of lipid reactive oxygen species (ROS), and the presence of iron is indispensable for the execution of ferroptosis.[7,9] Iron chelators such as deferoxamine (DFO) suppress ferroptosis by reducing the availability of iron; exogenous iron makes cells more sensitive to this cell death.[1,3] Moreover, genes and proteins that regulate iron metabolism, including its import, export, utilization, and storage, can modulate the ferroptosis sensitivity.[1−3,10−14] The process of selective autophagic turnover of ferritin (termed ferritinophagy) plays a crucial role in controlling iron homeostasis and is intimately involved in ferroptosis.

Ferritinophagy is mediated by nuclear receptor coactivator 4 (NCOA4), a recently identified autophagic cargo receptor.[15,16] Ferritin, consisting of 24 subunits of heavy (FTH1) and light (FTL) isoforms, is a cytosolic iron storage protein complex capable of chelating as many as 4500 iron atoms. By sequestering redox-active iron, ferritin plays an important antioxidant role in cells.[17,18] Recent studies demonstrate that ferritin is a key ferroptotic regulator, and its level affects the susceptibility to ferroptosis *in vitro* and *in vivo*.[19−21] In ferritinophagy, the cargo receptor NCOA4 directly recognizes and binds FTH1, then delivers iron-bound ferritin to autophagosomes for lysosomal degradation and iron release. It has been reported that ferritinophagy participates in ferroptosis. The knockdown of NCOA4 can inhibit ferritinophagy and block lipid peroxidation and ferroptosis by reducing the amount of bioavailable intracellular labile iron pools.[22,23]

Increasing evidence demonstrates that ferroptosis is implicated in the pathological cell death associated with many neurological diseases, including neurodegenerative disorders and strokes.[24−32] Blocking ferroptosis is considered to be a promising therapeutic strategy for these devastating diseases and has exhibited positive outcomes.[24−26]

Received: November 30, 2020
Published: May 6, 2021

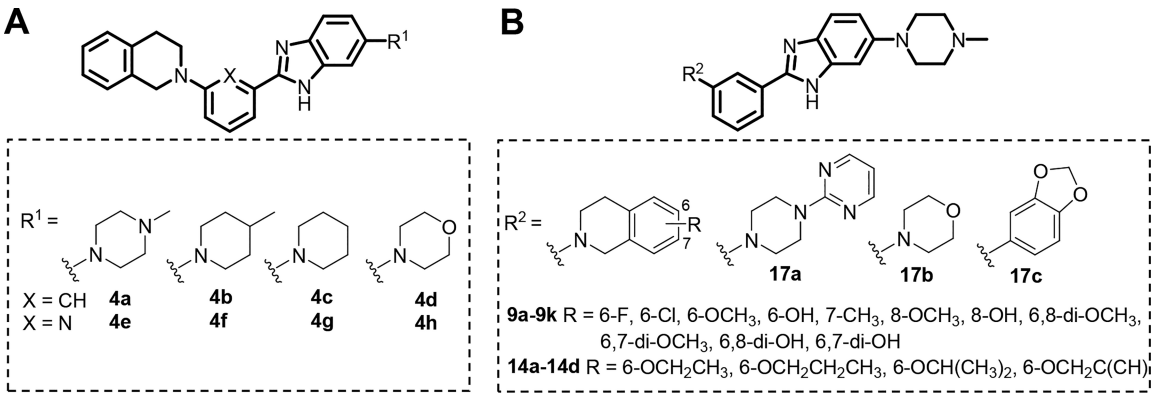

Figure 1. Structures of synthesized benzimidazole derivatives.

Previously, we reported that benzimidazole derivatives inhibited the system x_c^- inhibitor glutamate-induced ferroptosis in HT22 mouse hippocampal cells.[33] To further explore more potent ferroptosis inhibitors and the mechanism of action, we designed and synthesized a library of benzimidazole derivatives, which were assayed with Erastin-induced ferroptosis experiments. This resulted in the discovery of compound **9a**, a submicromolar ferroptosis inhibitor. In this work, **9a** is identified as the first ligand for NCOA4 and an inhibitor of the NCOA4−FTH1 interaction. It is demonstrated that developing inhibitors for the NCOA4−FTH1 interaction is a new strategy to halt ferroptosis and develop novel therapeutic solutions to combat neurological diseases, such as ischemic stroke.

RESULTS AND DISCUSSION

Discovery of a Potent Ferroptosis Inhibitor. In our earlier work, we identified ten benzimidazole derivatives with inhibitory activity against glutamate-induced ferroptosis in HT22 cells.[33] In this study, we further confirmed that these compounds also inhibited ferroptosis of HT22 cells induced by Erastin (another inhibitor of system x_c^-), as shown in Figure S1.

To explore the ferroptosis inhibitory activity space, we designed and synthesized a new library of benzimidazole derivatives (Figure 1A) by introducing lipophilic groups at R^1. The substituents at R^1 are cyclic amines (*N*-methylpiperazine, methylpiperazine, morpholine, and piperidine) to improve the solubility of the compound; the central aromatic ring is benzene or pyridine. This led to the first-generation library with eight compounds (**4a−h**). These compounds were tested for their inhibitory activities against Erastin-induced ferroptosis in HT22 cells, and the results are listed in Table 1.

In the first-generation library, **4a** was the most potent compound (EC_{50} = 0.50 μM). Therefore, a second-generation library was designed and synthesized based on **4a**. This resulted in 18 compounds (Figure 1B), and we discovered more compounds (**9a−b**, **9e−f**, and **14a−d**) whose activities were comparable to that of **4a**. Their antiferroptosis EC_{50} values are in the submicromolar range. The most potent compound, **9a**, was chosen for further antiferroptosis evaluation.

Cysteine depletion using a culture medium free of cystine can also induce ferroptosis. We found that the cotreatment of HT22 cells with **9a**, the classic ferroptosis inhibitor Fer-1, or DFO significantly reduced the level of cell death from cysteine depletion (Figure S2A). L-Buthionine sulfoximine (BSO), an inhibitor of the GSH synthetic enzyme γ-glutamate-cysteine ligase, depletes intracellular GSH, triggering ferroptosis.[2,7,8]

Table 1. Inhibitory Activities of Synthesized Compounds against Erastin-Induced Ferroptosis in HT22 Cells[a]

ID	R	EC_{50} (μM)	ID	R	EC_{50} (μM)
4a		0.50	**4b**		0.64
4c		1.21	**4d**		1.70
4e		0.78	**4f**		0.67
4g		n.d.	**4h**		n.d.
9a	6-F	0.29	**9b**	6-Cl	0.51
9c	6-OCH_3	1.01	**9d**	6-OH	n.d.
9e	7-CH_3	0.77	**9f**	8-OCH_3	0.33
9g	8-OH	n.d.	**9h**	6,8-di-OCH_3	n.d.
9i	6,7-di-OCH_3	1.44	**9j**	6,8-di-OH	n.d.
9k	6,7-di-OH	n.d.	**14a**	6-OCH_2CH_3	0.51
14b	6-$OCH_2CH_2CH_3$	0.39	**14c**	6-$OCH(CH_3)_2$	0.53
14d	6-$OCH_2C(CH)$	0.88			
17a		n.d.	**17b**		n.d.
17c		n.d.			
Fer-1		0.082	DFO		5.75

[a]n.d., cell viability was lower than 50% at 1.0 μM in cells cotreated with Erastin.

With the assay of BSO-induced ferroptosis in HT22 cells, we found that **9a** dose-dependently prevented cell death (Figure S2B). In addition, using either the assay of the GPX4 covalent inhibitor (1*S*,3*R*)-RSL3 (hereafter RSL3) or ML210-induced ferroptosis in HT22 cells, we demonstrated that **9a** had a ferroptosis inhibitory behavior similar to those of Fer-1 and DFO (Figures 2A and S2C, respectively). Morphologically, **9a** also protected HT22 cells from the damage triggered by RSL3 (Figure S2D). Furthermore, **9a** inhibited ferroptosis induced by Erastin, RSL3, or ML210 in HT-1080 human fibrosarcoma cells, another ferroptosis-sensitive cell line (Figure S2E). As shown in Figure 2B, **9a** also significantly suppressed ferroptosis induced by knockdown of GPX4 in HT-1080 cells.

Lipid peroxidation is the hallmark of ferroptosis. The levels of lipid ROS were measured with BODIPY 581/591 C11 (BODIPY-C11), a lipid peroxidation-sensitive dye, using confocal laser scanning microscopy and flow cytometry. In HT22 cells, RSL3 induced significant lipid ROS accumulation, which was indicated by the increase in the amount of oxidized BODIPY-C11 (green fluorescence). When cells were coincubated with RSL3 and either **9a** or Fer-1, the fluorescence intensity was remarkably decreased (Figures 2C and D). In addition, **9a** inhibited lipid ROS accumulation induced by the knockdown of GPX4 in HT-1080 cells (Figure S2F). The RSL3-

https://doi.org/10.1021/acscentsci.0c01592
ACS Cent. Sci. 2021, 7, 980−989

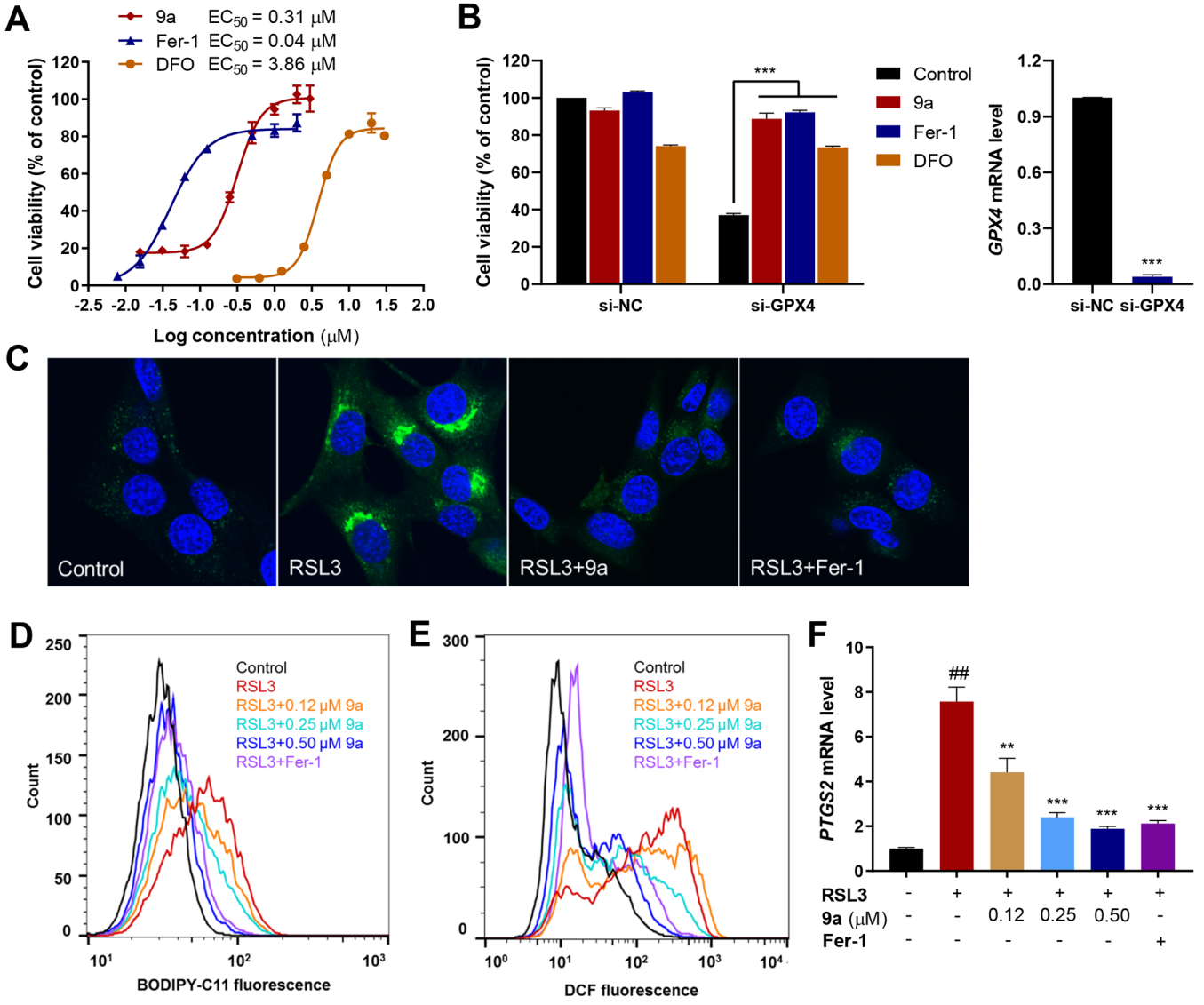

Figure 2. Compound **9a** inhibits ferroptosis. (A) Dose−response relationship for the inhibition of RSL3 (1 μM, 24 h)-induced death in HT22 cells by **9a** (red), Fer-1 (blue), and DFO (yellow). Cell viability was assayed using a cell counting kit-8 (CCK-8) kit. (B) Inhibitory activity of **9a** against ferroptosis induced by the knockdown of GPX4 in HT-1080 cells. Cells were transfected with scrambled siRNA (si-NC, negative control) or a GPX4-targeting siRNA (si-GPX4) for 12 h, then treated with or without 0.5 μM **9a**, 0.5 μM Fer-1, or 20 μM DFO for 36 h. Cell viability was assayed using a CCK-8 kit. Data shown represent the mean ± SEM from three independent experiments; ***$p < 0.001$. (C) Confocal imaging of oxidized BODIPY-C11 in HT22 cells treated with 1 μM RSL3 in the absence or presence of 0.5 μM **9a** or 0.5 μM Fer-1 for 3 h. Nuclei were stained with Hoechst 33342 (blue). Flow cytometry analyses of (D) lipid ROS levels and (E) cytosolic ROS levels in HT22 cells treated with the indicated stimuli for 3 h. (F) HT22 cells were treated as indicated for 12 h. *PTGS2* mRNA was measured by quantitative PCR (qPCR) with reverse transcription. Data shown represent the mean ± SEM from three independent experiments; $^{\#\#}p < 0.01$ compared with control cells, and **$p < 0.01$ and ***$p < 0.001$ compared with cells treated with RSL3 alone.

induced cytosolic ROS accumulation was also suppressed by **9a** in a dose-dependent manner in HT22 cells. This was detected by flow cytometry with 5- (and 6-) carboxy-2′,7′-dichlorodihydrofluorescein diacetate (carboxy-H_2DCFDA), a cytosolic ROS sensor (Figure 2E). The increased level of *PTGS2* mRNA expression induced by RSL3 is a marker for the lipid peroxidation that occurs during ferroptosis.[4,34] As shown in Figure 2F, **9a** dose-dependently inhibited the upregulation of *PTGS2* expression.

It should be noted that **9a** cannot inhibit staurosporine (STS)-induced apoptosis, hydrogen peroxide (H_2O_2)-induced necrosis, or TNF-α/SM-164/zVAD-fmk-induced necroptosis (Figure S2G). Together, these results demonstrate that **9a** is a selective ferroptosis inhibitor that effectively suppresses lipid peroxidation and rescues cells from ferroptosis.

Compound 9a Inhibits Ferroptosis by Decreasing the Amount of Intracellular Free Fe^{2+}. The aforementioned experiments revealed that **9a** suppressed ferroptosis induced by directly inactivating or depleting GPX4. Additionally, **9a** did not change the intracellular GSH level (Figure S3A) or GPX4 expression (Figures S3B and C). Therefore, **9a** probably inhibits ferroptosis downstream of or in parallel to GPX4. It has been reported that Fer-1 and liproxstatin-1 (Lip-1), the most commonly used ferroptosis inhibitors, suppress ferroptosis by acting as radical-trapping antioxidants (RTAs).[1,27,35] The 2,2-diphenyl-1-picrylhydrazyl (DPPH) assay under cell-free con-

https://doi.org/10.1021/acscentsci.0c01592
ACS Cent. Sci. 2021, 7, 980−989

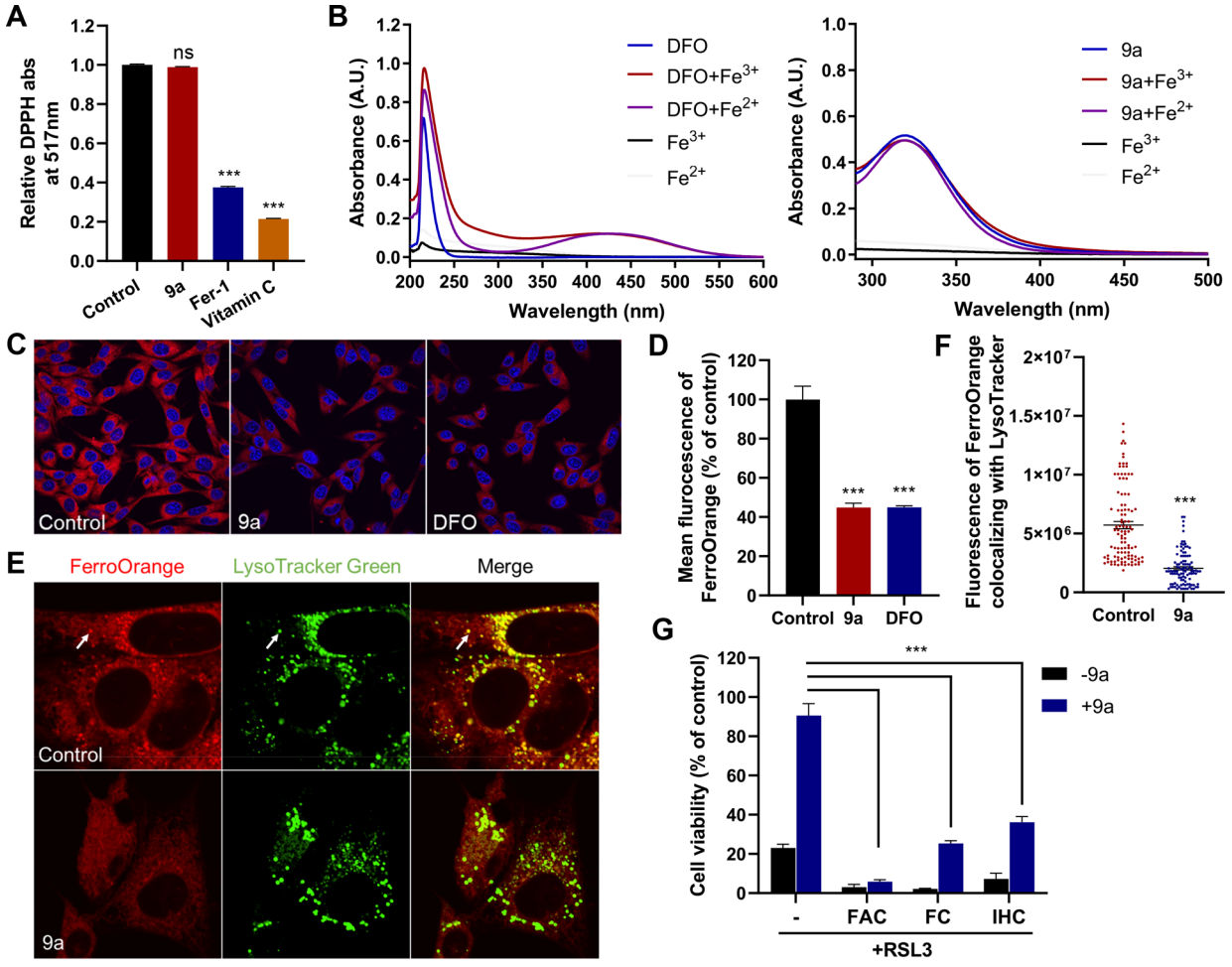

Figure 3. Compound **9a** reduces the amount of bioavailable ferrous iron to block ferroptosis. (A) Cell-free antioxidant potential monitored by changes in the absorbance at 517 nm of the stable radical DPPH. The concentration of all tested compounds was 50 μM. Data shown represent the mean ± SEM from three independent experiments; ns, not significant; ***$p < 0.001$. (B) UV−vis absorption spectra of DFO and **9a** in the absence or presence of Fe^{3+} or Fe^{2+}. (C) Confocal imaging of FerroOrange (red) in HT22 cells treated with 0.5 μM **9a** or 50 μM DFO for 6 h. Nuclei were stained with Hoechst 33342 (blue). (D) Quantification of the fluorescence intensity of FerroOrange. (E) Confocal imaging of FerroOrange (red) and LysoTracker Green (green) in HT22 cells treated with 0.5 μM **9a** for 6 h. The images show the subcellular localization of Fe^{2+} in live cells. LysoTracker Green stains the lysosomes. (F) Quantification of the fluorescence intensity of FerroOrange colocalized with LysoTracker Green per cell. Approximately 100 cells were measured per condition. (G) Cell viability of HT22 cells treated as indicated. In the absence or presence of 0.5 μM **9a**, cells were treated with 1 μM RSL3 ± 10 μg/mL ferric ammonium citrate (FAC), 25 μM ferric citrate (FC), or 20 μM iron chloride hexahydrate (IHC) for 12 h. (D, F, and G) Data shown represent the mean ± SEM from three independent experiments; ***$p < 0.001$.

ditions, however, demonstrated that **9a** cannot directly scavenge free radicals (Figure 3A), indicating that the compound was devoid of antioxidant activity. Since the iron chelator DFO is also a classic ferroptosis inhibitor, we tested the iron chelating properties of **9a** using UV−vis spectroscopy. As shown in Figure 3B, DFO displays a characteristic peak with a maximum absorption at ∼430 nm in the presence of irons.[36,37] However, no new peak was observed when adding irons to the solution of **9a**, suggesting that **9a** cannot chelate Fe^{3+} or Fe^{2+}. In spite of this, given the crucial role of ferrous iron in promoting lipid ROS formation and ferroptosis, we explored whether **9a** can alter the levels of available Fe^{2+} in live cells using the Fe^{2+}-selective fluorescent probe FerroOrange. Similar to that treated with DFO, the fluorescence intensity of FerroOrange in HT22 cells significantly decreased upon treatment with **9a** (Figures 3C and D), suggesting that **9a** reduced the level of free Fe^{2+}. Interestingly, it was also observed that the large quantity of Fe^{2+} in lysosomes (colocalization of FerroOrange and LysoTracker Green) was diminished when HT22 cells were treated with **9a** (Figures 3E and F). The number of lysosomes was not changed by **9a** (Figures S4A and B), precluding the possibility that the decrease in the amount of lysosomal Fe^{2+} was due to the decrease in the number of lysosomes. The reduction of the Fe^{2+} level induced by **9a** was also observed in HT-1080 cells, again without altering the number of lysosomes (Figures S4C−H).

To further confirm that **9a** suppresses ferroptosis by lowering the amount of bioavailable intracellular Fe^{2+}, we examined the effects of iron addition on the inhibitory activity of **9a** against ferroptosis. We found that treatment of HT22 cells with three different exogenous sources of iron (ferric ammonium citrate, ferric citrate, and iron chloride hexahydrate) abolished or significantly mitigated the ability of **9a** to rescue cells from RSL3-induced ferroptosis (Figure 3G). Because **9a** cannot bind irons, the induced decrease in Fe^{2+} level is most likely a result of the regulation of **9a** on iron metabolism.

Compound 9a Inhibits the Degradation of Ferritin Complexes in Lysosomes (Ferritinophagy) and Localizes

https://doi.org/10.1021/acscentsci.0c01592
ACS Cent. Sci. 2021, 7, 980−989

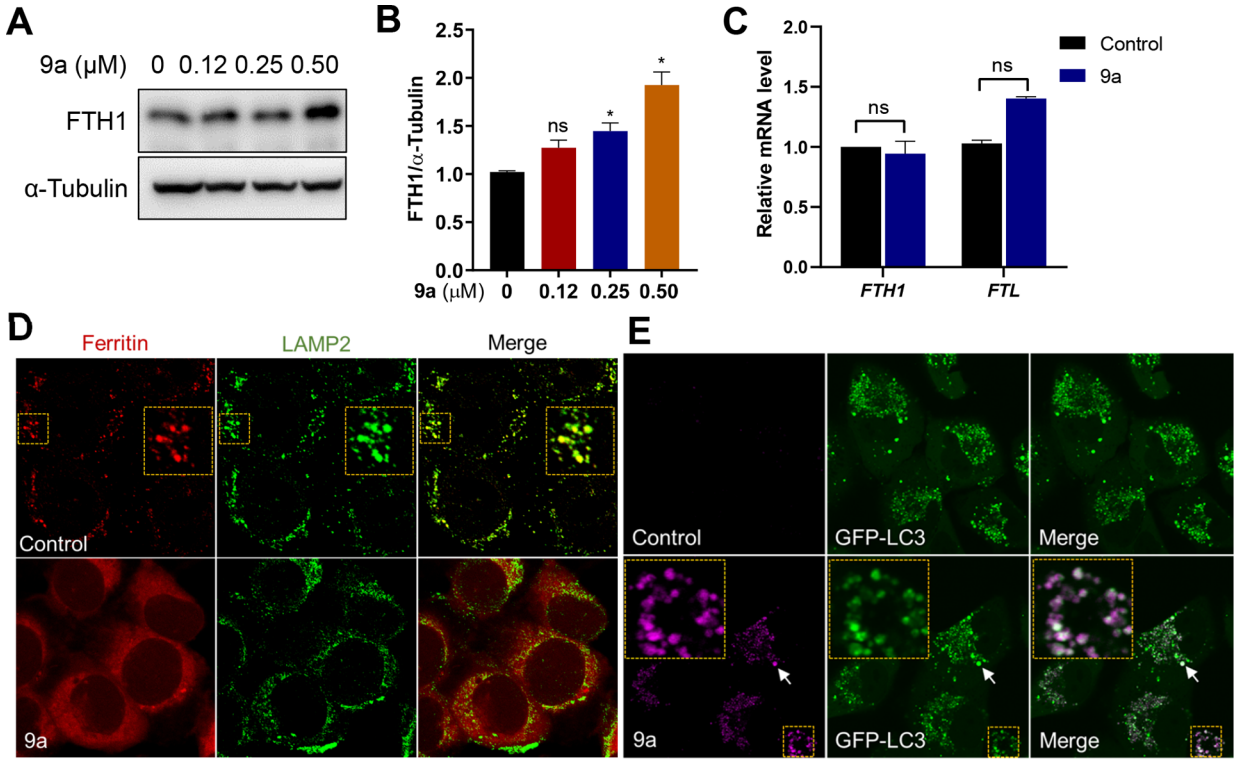

Figure 4. Compound **9a** inhibits lysosomal ferritin degradation and localizes in autophagosomes. (A) Immunoblot analysis of HT22 cells treated with the indicated concentrations of **9a** for 6 h. (B) Quantification of the immunoblot analysis in panel A. Data shown represent the mean ± SEM from three independent experiments; $*p < 0.05$. (C) Effects of **9a** on the mRNA levels of *FTH1* and *FTL*. HT22 cells were treated with 0.5 μM **9a** for 6 h. Data shown represent the mean ± SEM from three independent experiments. (D) Immunofluorescence imaging of ferritin (red) in HT-1080 cells treated with **9a**. LAMP2 (green) stains lysosomes. (E) Confocal imaging of **9a** (magenta) in A549 cells that stably expressed GFP-LC3 and were treated for 2 h with the compound at 10 μM. The colocalized foci are indicated by white arrows and shown in an enlarged image of the yellow box.

in Autophagosomes. As the major iron storage protein complex in mammals, ferritin plays a vital role in iron metabolism and protecting against ferroptosis. Large amounts of sequestered iron can be liberated from the ferritin complex via ferritinophagy, the process of the autophagic turnover of ferritin.[15,16,38] Because **9a** diminished the level of Fe^{2+} in lysosomes, we assumed that **9a** inhibits ferritinophagy. To prove this hypothesis, we first determined the levels of ferritin by Western blotting, and found that upon treatment with **9a**, the protein level of ferritin increased in a dose-dependent manner (Figures 4A and B). Additionally, using qPCR experiments, we revealed that **9a** did not change the mRNA expressions of *FTH1* and *FTL* (Figure 4C). Therefore, **9a** induced an increase in the amount of ferritin by inhibiting protein degradation, not by upregulating gene transcription.

To further validate that **9a** suppressed lysosomal ferritin degradation, we performed immunofluorescence experiments to observe the ferritin lysosomal localization. To promote ferritin accumulation in lysosomes, HT-1080 cells were loaded with FAC for 12 h, then incubated with DFO for 6 h in the presence of lysosomal protease inhibitors (E64-d and Pepstatin A). As previously reported, cells exhibited punctate ferritin lysosomal localization,[15,39] whereas the presence of **9a** led to diffuse ferritin staining (Figure 4D). This suggests that **9a** indeed blocks ferritin colocalization with lysosomes and causes impaired ferritinophagy.

Compound **9a** has a conjugated system with fluorescent emission (Figure S5A), and this characteristic was used to investigate its distribution in live cells. With confocal laser scanning microscopy, we observed that **9a** accumulated as punctate vesicles in the cytoplasm in both HT22 and HT-1080 cells, regardless of the presence of RSL3 (Figure S5B). Interestingly, the **9a** foci (magenta staining) well colocalized with the green fluorescent protein (GFP)-LC3 puncta (merged white staining, Figures 4E and S5C) in A549 human lung adenocarcinoma cells stably expressing GFP-fused LC3 protein (a marker of autophagosomes), suggesting that **9a** accumulated in autophagosomes. To further confirm this, the alkyne compound **14d** (a derivative of **9a**) with antiferroptosis activity was labeled by means of *in situ* click chemistry, and immunofluorescence staining was carried out. As shown in Figure S5F, **14d** also gave punctate cell labeling, and these foci colocalized with LC3. Again, this result supports that **9a** targets autophagosomes. In contrast, **9a** did not accumulate in the endoplasmic reticulum (ER) or mitochondria (Figure S6). To some extent, the localization of **9a** in autophagosomes indicates that **9a** interferes with ferritinophagy.

Compound 9a Inhibits Ferritinophagy by Disrupting the NCOA4−FTH1 Interaction through Binding to NCOA4 in Cells. Ferritinophagy is mediated by the cargo receptor NCOA4, which directly recognizes FTH1 and then transports the ferritin complex to autophagosomes for lysosomal degradation and iron release.[15,16] It is clear that the NCOA4−FTH1 protein−protein interaction (PPI) is essential for ferritinophagy. Therefore, with coimmunoprecipitation (co-IP) assays, we investigated whether **9a** abolished the NCOA4−FTH1 interaction to inhibit ferritinophagy. HEK-293T cells were transfected with Myc- and His-tagged FTH1 and Flag-tagged NCOA4, followed by DMSO or **9a** treatment for 16 h, and then a co-IP assay was performed. As shown in Figure 5A,

https://doi.org/10.1021/acscentsci.0c01592
ACS Cent. Sci. 2021, 7, 980−989

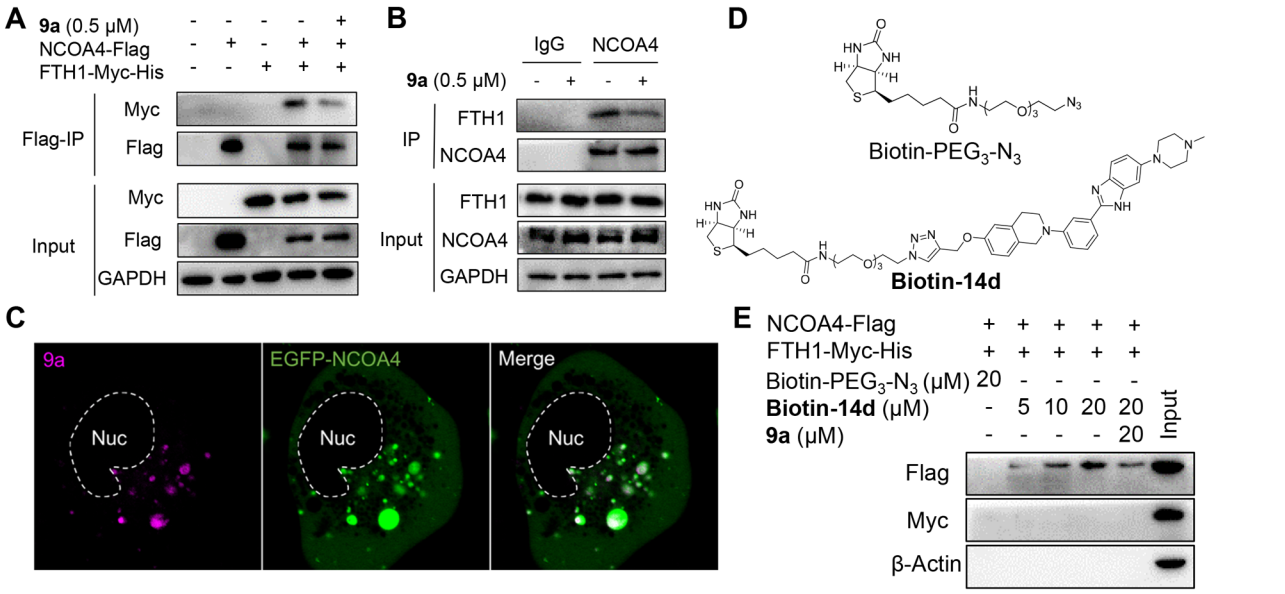

Figure 5. Compound **9a** disrupts the NCOA4−FTH1 interaction and binds to NCOA4. (A) Immunoprecipitation (IP) and immunoblot analysis of the interaction of FTH1-Myc-His and NCOA4-Flag in HEK-293T cells. **9a** was added at 8 h post-transfection. The lysates from HEK-293T cells expressing the indicated proteins were immunoprecipitated with anti-Flag (Flag-IP) and immunoblotted with the indicated antibodies. (B) IP and immunoblot analysis of the interaction of endogenous FTH1 and NCOA4 in HT-1080 cells treated with **9a** for 6 h. IgG was used as a negative control. (C) Live-cell imaging of **9a** (magenta) in HT-1080 cells expressing EGFP-NCOA4; Nuc, nucleus. (D) Structures of Biotin-PEG_3-N_3 and **Biotin-14d**. (E) Specific binding of **9a** to NCOA4. The lysates from HEK-293T cells expressing FTH1-Myc-His and NCOA4-Flag were pretreated with either **9a** or DMSO at 4 °C for 6 h and then incubated with increasing concentrations of **Biotin-14d** (precoupled with streptavidin magnetic beads) at 4 °C overnight, followed by pull-down with streptavidin magnetic beads. The precipitates were immunoblotted with the indicated antibodies. Biotin-PEG_3-N_3 was used as a negative control for **Biotin-14d**.

the NCOA4−FTH1 interaction was substantially impaired by **9a**. In addition, we detected the endogenous interaction between the two proteins in HT-1080 cells. Consistently, **9a** also inhibited the endogenous NCOA4 interaction with FTH1 (Figure 5B). These results demonstrate that **9a** is a potent inhibitor of the NCOA4−FTH1 interaction in cells. Furthermore, we examined the impact of **9a** on autophagy. In A549 cell line stably expressing GFP-LC3, the autophagy inhibitor chloroquine (CQ) significantly enhanced the number of GFP-LC3 puncta. While these A549 cells were treated with **9a**, the number of GFP-LC3 puncta remained nearly the same as that in the control cells even at a high concentration (Figures S7A and B), indicating that **9a** cannot promote the formation of GFP-LC3 puncta. In line with this, the Western blotting analysis revealed that, unlike CQ, **9a** had no ability to induce an increase in the LC3-II level in HT22 cells (Figures S7C and D). Taken together, these data indicate that **9a** is not an autophagy inhibitor. Additionally, these results exclude the possibility that **9a** inhibits ferritinophagy by affecting autophagy.

Since NCOA4 is an autophagic cargo receptor, we hypothesized that **9a** directly binds to NCOA4 instead of FTH1. To prove this, we tested whether **9a** colocalized with NCOA4 in live cells. HT-1080 cells were transfected with a plasmid expressing enhanced GFP (EGFP)-tagged NCOA4, incubated with **9a**, and then imaged directly. As shown in Figure 5C, the **9a** foci were almost completely located in EGFP-NCOA4 puncta, demonstrating that **9a** targets NCOA4 in live cells. Given the autophagosomal distribution of NCOA4 in the cytoplasm, this result also supports the localization of **9a** in autophagosomes, as demonstrated above.

To further confirm the binding of **9a** to NCOA4, we synthesized a biotin-tagged chemical probe by conjugating biotin-PEG_3-N_3 with the active alkyne compound **14d**. We found that the probe (named **Biotin-14d**) effectively blocks RSL3-induced ferroptosis in HT22 cells (EC_{50} = 3.66 μM). The activity is comparable to the activity of its parent **14d** (EC_{50} = 0.69 μM, Figure S7E). Therefore, biotin−streptavidin pull-down experiments were carried out using **Biotin-14d**. Cell lysates from HEK-293T cells expressing FTH1-Myc-His and NCOA4-Flag were incubated with different concentrations of **Biotin-14d** or free biotin-PEG_3-N_3. The mixture was precipitated with streptavidin magnetic beads, followed by immunoblotting with the corresponding antitag antibody. As shown in Figure 5E, only NCOA4 was specifically pulled down by **Biotin-14d** in a dose-dependent manner, and the binding of **Biotin-14d** and NCOA4 was competitively inhibited by **9a**. Overall, these results demonstrate that **9a** binds to NCOA4 and blocks its interaction with FTH1 in live cells, thereby inhibiting ferritinophagy.

Compound 9a Directly Binds NCOA4$^{383-522}$ Protein and Inhibits the NCOA4$^{383-522}$−FTH1 Interaction. It has been reported that NCOA4 associates with FTH1 via the fragment containing amino acids 383−522, and this region of NCOA4 (NCOA4$^{383-522}$) is also required for ferritinophagy in live cells.[39] Hence, we prepared and purified the recombinant human NCOA4$^{383-522}$ protein for further analysis. As shown in Figure 6A, the *in vitro* recombinant NCOA4$^{383-522}$ protein was pulled down by the synthesized biotin-tagged probe **Biotin-14d** in a dose-dependent manner, which was detected by silver staining and immunoblotting. Additionally, the binding of NCOA4$^{383-522}$ and **Biotin-14d** was blocked when the protein was preincubated with **9a**. Meanwhile, we did not detect the binding of **Biotin-14d** to recombinant human FTH1 protein. This result further confirms that **9a** specifically interacts with NCOA4$^{383-522}$. The binding affinity of **9a** to NCOA4$^{383-522}$ was measured with surface plasmon resonance (SPR). The

https://doi.org/10.1021/acscentsci.0c01592
ACS Cent. Sci. 2021, 7, 980−989

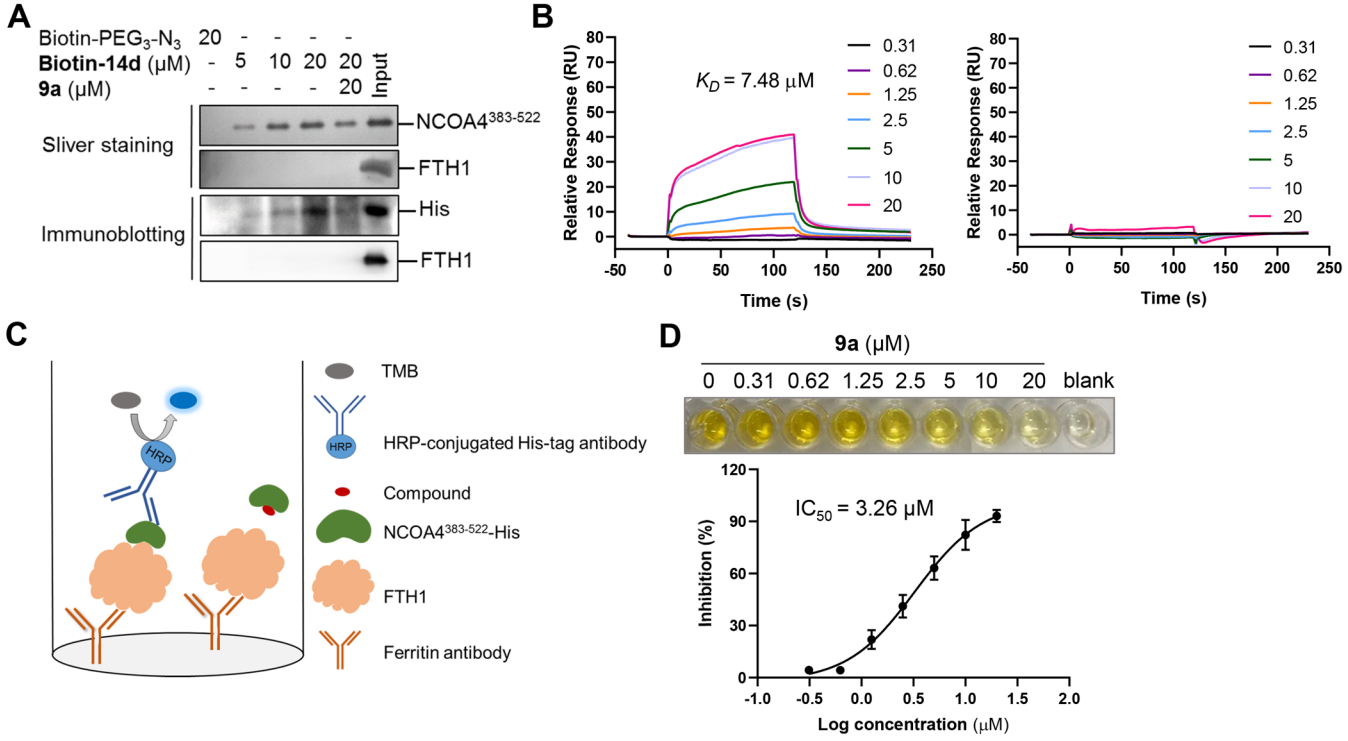

Figure 6. Compound **9a** directly binds NCOA4$^{383-522}$ and inhibits the NCOA4$^{383-522}$–FTH1 interaction. (A) Specific binding of **9a** to NCOA4$^{383-522}$. The recombinant NCOA4$^{383-522}$ or FTH1 protein was pretreated with **9a** or DMSO for 1 h and then incubated with increasing concentrations of **Biotin-14d** (precoupled with streptavidin magnetic beads) for 1 h. The proteins bound to the beads were detected by silver staining and Western blotting. (B) SPR sensorgrams for the binding of **9a** and the inactive compound **9h** to NCOA4$^{383-522}$. (C) Schematic of the ELISA assay used to detect the NCOA4$^{383-522}$–FTH1 interaction and its disruption by **9a**. (D) Dose–response relationship for the inhibition of the NCOA4$^{383-522}$–FTH1 interaction by **9a**. The indicated concentration of **9a** was preincubated with NCOA4$^{383-522}$, and the binding of NCOA4$^{383-522}$ to FTH1 was monitored by ELISA. Data shown represent the mean ± SEM from three independent experiments.

equilibrium dissociation constant (K_D) of the binding of **9a** to NCOA4$^{383-522}$ is 7.48 μM. As a negative control, the inactive compound **9h** has no binding to the recombinant protein (Figure 6B). Moreover, to confirm that **9a** directly inhibits the NCOA4$^{383-522}$–FTH1 interaction, we developed an enzyme-linked immunosorbent assay (ELISA) to detect NCOA4$^{383-522}$ binding to FTH1 protein (a schematic is shown in Figure 6C). In this assay, **9a** significantly disrupted the NCOA4–FTH1 interaction (IC_{50} = 3.26 μM), as shown in Figure 6D.

Compound 9a Alleviates Cerebral Ischemic Injury in Rats Subjected to Transient Middle Cerebral Artery Occlusion (MCAO). Ischemic stroke occurs as a result of vascular occlusion and is the most common form of stroke, which is a leading cause of death and permanent disability. To date, there is no effective therapy for this disease.[26,40] Current studies indicate that ferroptotic pathways have been involved in the pathological process of ischemic stroke, and the inhibition of ferroptosis can ameliorate ischemic brain injury *in vivo*.[1,24,26,41,42]

Since **9a** has a pronounced inhibitory activity against ferroptosis in cells, we evaluated whether **9a** can be protective *in vivo* in a MCAO model of ischemic stroke. In this model, rats were given **9a** (10 mg/kg), Fer-1 (10 mg/kg), or vehicle by intraperitoneal injection. A filament suture was used to occlude the middle cerebral artery for 1.5 h and then withdrawn for reperfusion. The results from brain sections stained with 2,3,5-tripenyltetrazolium chloride (TTC) showed that, similar to Fer-1, **9a** also substantially reduced infarct volume at 24 h post reperfusion (Figures 7A and B). Additionally, the Longa test indicated that **9a** administration improved neurological deficits following focal ischemia (Figure 7C). The protection of **9a** against cerebral ischemic injury was also confirmed by histological observations, including H&E and Nissl staining (Figure 7D). For example, compared to normal cells with a regular shape and even staining, many neurons in the cortex of the lesioned hemisphere from MCAO-treated rats were shrunken with aberrant morphology, as indicated by Nissl staining. Strikingly, **9a** treatment maintained most neuronal cells in a regular shape and reduced the percentage of injured neurons in the cortex (Figure 7E).

In this model, we also detected the expression of *PTGS2* mRNA, a marker for the assessment of ferroptosis *in vivo*.[4] As shown in Figure 7F, **9a** significantly decreased the gene expression of *PTGS2* in the lesioned hemisphere. Moreover, **9a** reduced the levels of malondialdehyde (MDA) and 4-hydroxynonenal (4-HNE), two characteristic products of lipid peroxidation (Figure 7G). Together, *in vivo* data demonstrate that **9a** effectively alleviates cerebral ischemic damage through inhibiting ferroptosis.

CONCLUSIONS

In this work, a new and potent ferroptosis inhibitor **9a** was identified through phenotypic screening and structural modification. Systematic investigations reveal that through inhibiting ferritinophagy, **9a** lowers the level of intracellular labile Fe^{2+}, leading to ferroptosis suppression. This mechanism is distinct from that of the existing ferroptosis inhibitors Fer-1 and DFO. It was observed that **9a** accumulates in autophagosomes and

https://doi.org/10.1021/acscentsci.0c01592
ACS Cent. Sci. 2021, 7, 980–989

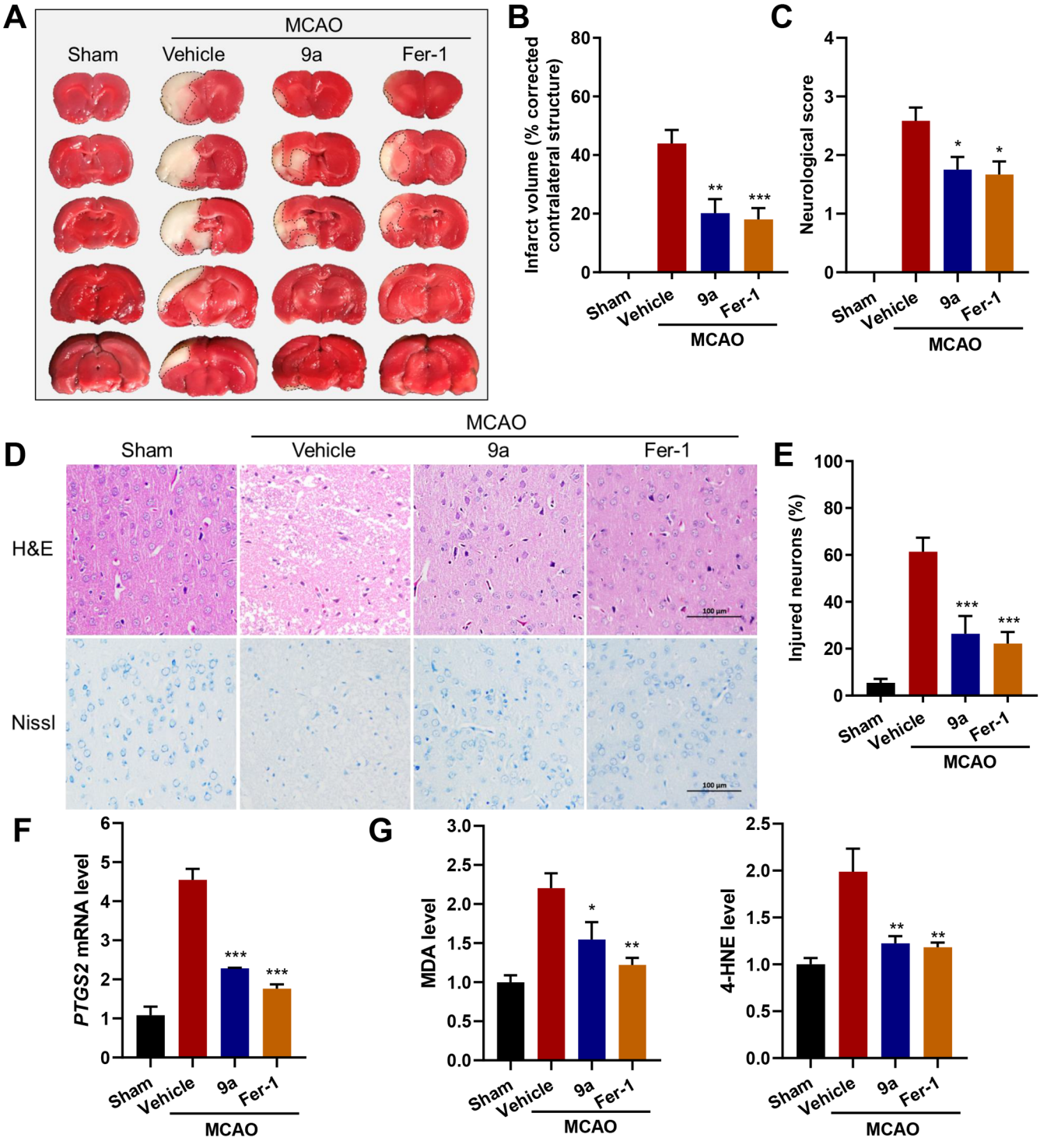

Figure 7. The administration of **9a** ameliorates ischemic reperfusion injury in the MCAO model. (A) Representative images of TTC staining in brain sections at 24 h after MCAO and reperfusion. The infarction area is indicated by the white color with a black outline. Either **9a** or Fer-1 was injected into rats 0.5 h before and 2 h after the MCAO occlusion. (B) Quantification of the infarction volume (corrected by the contralateral structure) as indicated by TTC staining using ImageJ (n = 8–9). (C) Statistical analysis of the neurological score (higher numbers indicate more severe impairment) in the Longa test performed at 24 h after MCAO and reperfusion (n = 12). (D) Representative images of H&E (hematoxylin and eosin) and Nissl staining of the cortex of the lesioned hemisphere. The scale bar is 100 μm. (E) Quantification of the percentage of injured neurons in the cortex of the lesioned hemisphere (n = 6). (F) Relative *PTGS2* mRNA, (G) MDA, and 4-HNE levels in the lesioned hemisphere (n = 6). Data shown represent the mean ± SEM; *p < 0.05, **p < 0.01, and ***p < 0.001 compared with the group treated with vehicle.

colocalizes with the autophagic receptor NCOA4 in live cells. With the synthesized probe **Biotin-14d**, NCOA4 was further identified as the target of **9a**. Through binding to NCOA4, compound **9a** disrupts the NCOA4−FTH1 interaction and then blocks NCOA4-dependent ferritinophagy. We also demonstrate that **9a** directly binds to NCOA4 *in vitro* with the purified

https://doi.org/10.1021/acscentsci.0c01592
ACS Cent. Sci. 2021, 7, 980−989

ferritin-binding domain of human NCOA4, fragment 383−522 (NCOA4$^{383-522}$). Moreover, the inhibition of **9a** in regard to the NCOA4$^{383-522}$−FTH1 interaction was confirmed in a developed ELISA assay. As an effective ferroptosis inhibitor, **9a** protects brain from ischemic reperfusion injury in rats subjected to MCAO.

With the first ligand **9a**, this study uncovers that NCOA4 is a potential drug target. Moreover, this work demonstrates that the interaction of NCOA4 and iron-bound ferritin is important for ferroptosis. Gene-depleting NCOA4 can inhibit ferritinophagy and ferroptosis, as previously reported;[22,23] blocking the NCOA4−FTH1 interaction with small molecules can also hinder this selective autophagy process, leading to a decrease in the amount of bioavailable Fe^{2+} as well as ferroptosis suppression, as revealed in this work. To our best knowledge, **9a** is the first NCOA4−FTH1 protein−protein interaction inhibitor. This study indicates that except for certain enzymes associated with lipid metabolism, such as GPX4, acyl-CoA synthetase long-chain family member 4 (ACSL4), and lipoxygenases (LOXs), the NCOA4−FTH1 interaction is also a key target when developing new ferroptosis inhibitors.

■ ASSOCIATED CONTENT

Supporting Information

The Supporting Information is available free of charge at https://pubs.acs.org/doi/10.1021/acscentsci.0c01592.

Experimental details and NMR spectra (PDF)

■ AUTHOR INFORMATION

Corresponding Authors

Qiong Gu − *Research Center for Drug Discovery, School of Pharmaceutical Sciences, Sun Yat-sen University, Guangzhou 510006, China;* orcid.org/0000-0001-6011-3697; Email: guqiong@mail.sysu.edu.cn

Jun Xu − *Research Center for Drug Discovery, School of Pharmaceutical Sciences, Sun Yat-sen University, Guangzhou 510006, China;* orcid.org/0000-0002-1075-0337; Email: junxu@biochemomes.com

Authors

Yuying Fang − *Research Center for Drug Discovery, School of Pharmaceutical Sciences, Sun Yat-sen University, Guangzhou 510006, China*

Xiucai Chen − *Research Center for Drug Discovery, School of Pharmaceutical Sciences, Sun Yat-sen University, Guangzhou 510006, China*

Qingyun Tan − *Research Center for Drug Discovery, School of Pharmaceutical Sciences, Sun Yat-sen University, Guangzhou 510006, China*

Huihao Zhou − *Research Center for Drug Discovery, School of Pharmaceutical Sciences, Sun Yat-sen University, Guangzhou 510006, China;* orcid.org/0000-0002-9675-5007

Complete contact information is available at: https://pubs.acs.org/10.1021/acscentsci.0c01592

Notes

The authors declare no competing financial interest.

■ ACKNOWLEDGMENTS

This work was supported by the National Key R&D Program of China (2017YFB02034043) and the Science and Technology Planning Project of Guangdong Province (2016A020217005). We thank Dr. Min Li (School of Pharmaceutical Sciences, Sun Yat-sen University) for kindly providing A549 cells that stably expressed GFP-LC3 and the Jianwen Chen team (New Drug R&D Technology Center, School of Pharmaceutical Science, Sun Yat-sen University) for assistance during the *in vivo* surgery.

■ REFERENCES

(1) Dixon, S. J.; Lemberg, K. M.; Lamprecht, M. R.; Skouta, R.; Zaitsev, E. M.; Gleason, C. E.; Patel, D. N.; Bauer, A. J.; Cantley, A. M.; Yang, W. S.; Morrison, B.; Stockwell, B. R. Ferroptosis: an iron-dependent form of nonapoptotic cell death. *Cell* **2012**, *149*, 1060−1072.

(2) Stockwell, B. R.; Friedmann Angeli, J. P.; Bayir, H.; Bush, A. I.; Conrad, M.; Dixon, S. J.; Fulda, S.; Gascon, S.; Hatzios, S. K.; Kagan, V. E.; Noel, K.; Jiang, X.; Linkermann, A.; Murphy, M. E.; Overholtzer, M.; Oyagi, A.; Pagnussat, G. C.; Park, J.; Ran, Q.; Rosenfeld, C. S.; Salnikow, K.; Tang, D.; Torti, F. M.; Torti, S. V.; Toyokuni, S.; Woerpel, K. A.; Zhang, D. D. Ferroptosis: a regulated cell death nexus linking metabolism, redox biology, and disease. *Cell* **2017**, *171*, 273−285.

(3) Hassannia, B.; Vandenabeele, P.; Vanden Berghe, T. Targeting ferroptosis to iron out cancer. *Cancer Cell* **2019**, *35*, 830−849.

(4) Yang, W. S.; SriRamaratnam, R.; Welsch, M. E.; Shimada, K.; Skouta, R.; Viswanathan, V. S.; Cheah, J. H.; Clemons, P. A.; Shamji, A. F.; Clish, C. B.; Brown, L. M.; Girotti, A. W.; Cornish, V. W.; Schreiber, S. L.; Stockwell, B. R. Regulation of ferroptotic cancer cell death by GPX4. *Cell* **2014**, *156*, 317−331.

(5) Friedmann Angeli, J. P.; Schneider, M.; Proneth, B.; Tyurina, Y. Y.; Tyurin, V. A.; Hammond, V. J.; Herbach, N.; Aichler, M.; Walch, A.; Eggenhofer, E.; Basavarajappa, D.; Radmark, O.; Kobayashi, S.; Seibt, T.; Beck, H.; Neff, F.; Esposito, I.; Wanke, R.; Forster, H.; Yefremova, O.; Heinrichmeyer, M.; Bornkamm, G. W.; Geissler, E. K.; Thomas, S. B.; Stockwell, B. R.; O'Donnell, V. B.; Kagan, V. E.; Schick, J. A.; Conrad, M. Inactivation of the ferroptosis regulator Gpx4 triggers acute renal failure in mice. *Nat. Cell Biol.* **2014**, *16*, 1180−1191.

(6) Koppula, P.; Zhang, Y.; Zhuang, L.; Gan, B. Amino acid transporter SLC7A11/xCT at the crossroads of regulating redox homeostasis and nutrient dependency of cancer. *Cancer commun (London, England)* **2018**, *38*, 12−24.

(7) Dixon, S. J.; Stockwell, B. R. The hallmarks of ferroptosis. *Annu. Rev. Cancer Biol.* **2019**, *3*, 35−54.

(8) Cao, J. Y.; Dixon, S. J. Mechanisms of ferroptosis. *Cell. Mol. Life Sci.* **2016**, *73*, 2195−2209.

(9) Stockwell, B. R.; Jiang, X. A physiological function for ferroptosis in tumor suppression by the immune system. *Cell Metab.* **2019**, *30*, 14−15.

(10) Alvarez, S. W.; Sviderskiy, V. O.; Terzi, E. M.; Papagiannakopoulos, T.; Moreira, A. L.; Adams, S.; Sabatini, D. M.; Birsoy, K.; Possemato, R. NFS1 undergoes positive selection in lung tumours and protects cells from ferroptosis. *Nature* **2017**, *551*, 639−643.

(11) Hassannia, B.; Wiernicki, B.; Ingold, I.; Qu, F.; Van Herck, S.; Tyurina, Y. Y.; Bayir, H.; Abhari, B. A.; Angeli, J. P. F.; Choi, S. M.; Meul, E.; Heyninck, K.; Declerck, K.; Chirumamilla, C. S.; Lahtela-Kakkonen, M.; Van Camp, G.; Krysko, D. V.; Ekert, P. G.; Fulda, S.; De Geest, B. G.; Conrad, M.; Kagan, V. E.; Vanden Berghe, W.; Vandenabeele, P.; Vanden Berghe, T. Nano-targeted induction of dual ferroptotic mechanisms eradicates high-risk neuroblastoma. *J. Clin. Invest.* **2018**, *128*, 3341−3355.

(12) Ma, S.; Henson, E. S.; Chen, Y.; Gibson, S. B. Ferroptosis is induced following siramesine and lapatinib treatment of breast cancer cells. *Cell Death Dis.* **2016**, *7*, e2307−e2317.

(13) Sun, X.; Ou, Z.; Xie, M.; Kang, R.; Fan, Y.; Niu, X.; Wang, H.; Cao, L.; Tang, D. HSPB1 as a novel regulator of ferroptotic cancer cell death. *Oncogene* **2015**, *34*, 5617−5625.

(14) Yuan, H.; Li, X.; Zhang, X.; Kang, R.; Tang, D. CISD1 inhibits ferroptosis by protection against mitochondrial lipid peroxidation. *Biochem. Biophys. Res. Commun.* **2016**, *478*, 838−844.

(15) Mancias, J. D.; Wang, X.; Gygi, S. P.; Harper, J. W.; Kimmelman, A. C. Quantitative proteomics identifies NCOA4 as the cargo receptor mediating ferritinophagy. *Nature* **2014**, *509*, 105−109.
(16) Dowdle, W. E.; Nyfeler, B.; Nagel, J.; Elling, R. A.; Liu, S.; Triantafellow, E.; Menon, S.; Wang, Z.; Honda, A.; Pardee, G.; Cantwell, J.; Luu, C.; Cornella-Taracido, I.; Harrington, E.; Fekkes, P.; Lei, H.; Fang, Q.; Digan, M. E.; Burdick, D.; Powers, A. F.; Helliwell, S. B.; D'Aquin, S.; Bastien, J.; Wang, H.; Wiederschain, D.; Kuerth, J.; Bergman, P.; Schwalb, D.; Thomas, J.; Ugwonali, S.; Harbinski, F.; Tallarico, J.; Wilson, C. J.; Myer, V. E.; Porter, J. A.; Bussiere, D. E.; Finan, P. M.; Labow, M. A.; Mao, X.; Hamann, L. G.; Manning, B. D.; Valdez, R. A.; Nicholson, T.; Schirle, M.; Knapp, M. S.; Keaney, E. P.; Murphy, L. O. Selective VPS34 inhibitor blocks autophagy and uncovers a role for NCOA4 in ferritin degradation and iron homeostasis in vivo. *Nat. Cell Biol.* **2014**, *16*, 1069−1079.
(17) Pantopoulos, K.; Porwal, S. K.; Tartakoff, A.; Devireddy, L. Mechanisms of mammalian iron homeostasis. *Biochemistry* **2012**, *51*, 5705−5724.
(18) Masaldan, S.; Bush, A. I.; Devos, D.; Rolland, A. S.; Moreau, C. Striking while the iron is hot: Iron metabolism and ferroptosis in neurodegeneration. *Free Radical Biol. Med.* **2019**, *133*, 221−233.
(19) Tian, Y.; Lu, J.; Hao, X.; Li, H.; Zhang, G.; Liu, X.; Li, X.; Zhao, C.; Kuang, W.; Chen, D.; Zhu, M. FTH1 inhibits ferroptosis through ferritinophagy in the 6-OHDA model of Parkinson's disease. *Neurotherapeutics* **2020**, *17*, 1796−1812.
(20) Rui, T.; Wang, H.; Li, Q.; Cheng, Y.; Gao, Y.; Fang, X.; Ma, X.; Chen, G.; Gao, C.; Gu, Z.; Song, S.; Zhang, J.; Wang, C.; Wang, Z.; Wang, T.; Zhang, M.; Min, J.; Chen, X.; Tao, L.; Wang, F.; Luo, C. Deletion of ferritin H in neurons counteracts the protective effect of melatonin against traumatic brain injury-induced ferroptosis. *J. Pineal Res.* **2021**, *70*, e12704.
(21) Fang, X.; Cai, Z.; Wang, H.; Han, D.; Cheng, Q.; Zhang, P.; Gao, F.; Yu, Y.; Song, Z.; Wu, Q.; An, P.; Huang, S.; Pan, J.; Chen, H. Z.; Chen, J.; Linkermann, A.; Min, J.; Wang, F. Loss of cardiac ferritin H facilitates cardiomyopathy via Slc7a11-mediated ferroptosis. *Circ. Res.* **2020**, *127*, 486−501.
(22) Hou, W.; Xie, Y.; Song, X.; Sun, X.; Lotze, M. T.; Zeh, H. J., 3rd; Kang, R.; Tang, D. Autophagy promotes ferroptosis by degradation of ferritin. *Autophagy* **2016**, *12*, 1425−1428.
(23) Gao, M.; Monian, P.; Pan, Q.; Zhang, W.; Xiang, J.; Jiang, X. Ferroptosis is an autophagic cell death process. *Cell Res.* **2016**, *26*, 1021−1032.
(24) Alim, I.; Caulfield, J. T.; Chen, Y.; Swarup, V.; Geschwind, D. H.; Ivanova, E.; Seravalli, J.; Ai, Y.; Sansing, L. H.; Ste.Marie, E. J.; Hondal, R. J.; Mukherjee, S.; Cave, J. W.; Sagdullaev, B. T.; Karuppagounder, S. S.; Ratan, R. R. Selenium drives a transcriptional adaptive program to block ferroptosis and treat stroke. *Cell* **2019**, *177*, 1262−1279.
(25) Skouta, R.; Dixon, S. J.; Wang, J.; Dunn, D. E.; Orman, M.; Shimada, K.; Rosenberg, P. A.; Lo, D. C.; Weinberg, J. M.; Linkermann, A.; Stockwell, B. R. Ferrostatins inhibit oxidative lipid damage and cell death in diverse disease models. *J. Am. Chem. Soc.* **2014**, *136*, 4551−4556.
(26) Tuo, Q. Z.; Lei, P.; Jackman, K. A.; Li, X. L.; Xiong, H.; Li, X. L.; Liuyang, Z. Y.; Roisman, L.; Zhang, S. T.; Ayton, S.; Wang, Q.; Crouch, P. J.; Ganio, K.; Wang, X. C.; Pei, L.; Adlard, P. A.; Lu, Y. M.; Cappai, R.; Wang, J. Z.; Liu, R.; Bush, A. I. Tau-mediated iron export prevents ferroptotic damage after ischemic stroke. *Mol. Psychiatry* **2017**, *22*, 1520−1530.
(27) Angeli, J. P. F.; Shah, R.; Pratt, D. A.; Conrad, M. Ferroptosis inhibition: mechanisms and opportunities. *Trends Pharmacol. Sci.* **2017**, *38*, 489−498.
(28) Li, Q.; Han, X.; Lan, X.; Gao, Y.; Wan, J.; Durham, F.; Cheng, T.; Yang, J.; Wang, Z.; Jiang, C.; Ying, M.; Koehler, R. C.; Stockwell, B. R.; Wang, J. Inhibition of neuronal ferroptosis protects hemorrhagic brain. *JCI Insight* **2017**, *2*, e90777.
(29) Zille, M.; Karuppagounder, S. S.; Chen, Y.; Gough, P. J.; Bertin, J.; Finger, J.; Milner, T. A.; Jonas, E. A.; Ratan, R. R. Neuronal death after hemorrhagic stroke in vitro and in vivo shares features of ferroptosis and necroptosis. *Stroke* **2017**, *48*, 1033−1043.
(30) Chen, L.; Hambright, W. S.; Na, R.; Ran, Q. Ablation of the ferroptosis inhibitor glutathione peroxidase 4 in neurons results in rapid motor neuron degeneration and paralysis. *J. Biol. Chem.* **2015**, *290*, 28097−28106.
(31) Weiland, A.; Wang, Y.; Wu, W.; Lan, X.; Han, X.; Li, Q.; Wang, J. Ferroptosis and its role in diverse brain diseases. *Mol. Neurobiol.* **2019**, *56*, 4880−4893.
(32) Do Van, B.; Gouel, F.; Jonneaux, A.; Timmerman, K.; Gele, P.; Petrault, M.; Bastide, M.; Laloux, C.; Moreau, C.; Bordet, R.; Devos, D.; Devedjian, J. C. Ferroptosis, a newly characterized form of cell death in Parkinson's disease that is regulated by PKC. *Neurobiol. Dis.* **2016**, *94*, 169−178.
(33) Fang, Y.; Zhou, H.; Gu, Q.; Xu, J. Synthesis and evaluation of tetrahydroisoquinoline-benzimidazole hybrids as multifunctional agents for the treatment of Alzheimer's disease. *Eur. J. Med. Chem.* **2019**, *167*, 133−145.
(34) Fang, X.; Wang, H.; Han, D.; Xie, E.; Yang, X.; Wei, J.; Gu, S.; Gao, F.; Zhu, N.; Yin, X.; Cheng, Q.; Zhang, P.; Dai, W.; Chen, J.; Yang, F.; Yang, H. T.; Linkermann, A.; Gu, W.; Min, J.; Wang, F. Ferroptosis as a target for protection against cardiomyopathy. *Proc. Natl. Acad. Sci. U. S. A.* **2019**, *116*, 2672−2680.
(35) Zilka, O.; Shah, R.; Li, B.; Friedmann Angeli, J. P.; Griesser, M.; Conrad, M.; Pratt, D. A. On the mechanism of cytoprotection by Ferrostatin-1 and Liproxstatin-1 and the role of lipid peroxidation in ferroptotic cell death. *ACS Cent. Sci.* **2017**, *3*, 232−243.
(36) Liu, Z.; Qiao, J.; Nagy, T.; Xiong, M. P. ROS-triggered degradable iron-chelating nanogels: Safely improving iron elimination in vivo. *J. Controlled Release* **2018**, *283*, 84−93.
(37) Yu, B.; Yang, Y.; Liu, Q.; Zhan, A.; Yang, Y.; Liu, H. A novel star like eight-arm polyethylene glycol-deferoxamine conjugate for iron overload therapy. *Pharmaceutics* **2020**, *12*, 329−341.
(38) Zhou, B.; Liu, J.; Kang, R.; Klionsky, D. J.; Kroemer, G.; Tang, D. Ferroptosis is a type of autophagy-dependent cell death. *Semin. Cancer Biol.* **2020**, *66*, 89−100.
(39) Mancias, J. D.; Pontano Vaites, L.; Nissim, S.; Biancur, D. E.; Kim, A. J.; Wang, X.; Liu, Y.; Goessling, W.; Kimmelman, A. C.; Harper, J. W. Ferritinophagy via NCOA4 is required for erythropoiesis and is regulated by iron dependent HERC2-mediated proteolysis. *eLife* **2015**, *4*, e10308.
(40) Langhorne, P.; Bernhardt, J.; Kwakkel, G. Stroke rehabilitation. *Lancet* **2011**, *377*, 1693−1702.
(41) Yigitkanli, K.; Pekcec, A.; Karatas, H.; Pallast, S.; Mandeville, E.; Joshi, N.; Smirnova, N.; Gazaryan, I.; Ratan, R. R.; Witztum, J. L.; Montaner, J.; Holman, T. R.; Lo, E. H.; van Leyen, K. Inhibition of 12/15-lipoxygenase as therapeutic strategy to treat stroke. *Ann. Neurol.* **2013**, *73*, 129−135.
(42) Yang, W.; Liu, X.; Song, C.; Ji, S.; Yang, J.; Liu, Y.; You, J.; Zhang, J.; Huang, S.; Cheng, W.; Shao, Z.; Li, L.; Yang, S. Structure-activity relationship studies of phenothiazine derivatives as a new class of ferroptosis inhibitors together with the therapeutic effect in an ischemic stroke model. *Eur. J. Med. Chem.* **2021**, *209*, 112842−112862.

https://doi.org/10.1021/acscentsci.0c01592
ACS Cent. Sci. 2021, 7, 980−989